RSC Advances

PAPER

View Article Online
View Journal | View Issue

Check for updates

Cite this: *RSC Adv.*, 2022, **12**, 3847

Facile synthesis of silver nanocatalyst decorated Fe_3O_4@PDA core–shell nanoparticles with enhanced catalytic properties and selectivity†

Yujie Liu,[a] Haijun Zhou,*[a] Jinling Wang,[a] Ding Yu,[a] Zhaolei Li[a] and Rui Liu*[b]

Received 20th December 2021
Accepted 24th January 2022

DOI: 10.1039/d1ra09187e

rsc.li/rsc-advances

In this work, we have successfully prepared core–shell nanoparticles (Fe_3O_4@PDA) wrapped with Ag using a simple and green synthesis method. Without an external reducing agent, silver nanoparticles (Ag NPs) with good dispersibility were directly reduced and deposited on a polydopamine (PDA) layer. Fe_3O_4@PDA@Ag showed excellent catalytic activity and recyclability for 4-nitrophenol, and also exhibited good catalytic selectivity for organic dyes (MO and MB). This simple and green synthesis method will provide a platform for other catalytic applications.

1. Introduction

4-Nitrophenol (4-NP), as one of the main sources of pollution in modern industrial wastewater, is considered to be an important threat to the environment and human health.[1,2] Therefore, timely removal of pollutants in water is of great significance to environmental health and human sustainable development. As a treatment method of 4-nitrophenol, catalysis can not only promote the rapid and efficient degradation of 4-NP, but also produce 4-aminophenol,[3] an important chemical raw material. In addition, the cationic dye methylene blue (MB) and the anionic dye methyl orange (MO) are two typical organic dyes that pose a great threat to both ecosystems and human health too. Therefore, it has become urgent to find methods for fast and efficient treatment of organic dyes. Compared to other methods (such as adsorption, ozonation, and biodegradation),[4–7] catalysis has significant advantages. In the catalytic reduction of organic dyes, it has been reported that noble metal nanochemistry (*e.g.* Pt, Pd, Au, Ag)[8–11] has shown excellent catalytic activity.

Silver nanoparticles (Ag NPs) in various kinds of catalytic reactions are highly stable and efficient,[12–14] and Ag NPs are favored by industrial production due to lower production costs compared to other noble metal nanometals (*e.g.* gold, platinum, palladium). However, silver nanoparticles have a strong tendency to reduce specific surface area and form large aggregates, which will reduce surface active sites and catalytic performance.[15] Therefore, avoid of aggregation and preparing Ag NPs particles with good monodispersity have become the priority tasks of preparing highly efficient and stable nanocatalysts. In the past few decades, the immobilization of nanoparticles in carriers (such as activated carbon, ZIF8, graphene, polymers)[16–19] has been used to solve the above problems.

Polydopamine (PDA) has attracted attention because of its ability to coat almost all kinds of materials and its unique functionality.[20] Polydopamine molecular chains are rich in many phenolic hydroxyl and amino functional groups, which are highly chemically active and can be surface modified to achieve a wide range of applications for PDA functional materials.[21,22] The addition of Fe_3O_4 not only can enable rapid recycling and reusing of catalytic materials, but also provide a template for DA polymerization and form the Fe_3O_4@PDA core–shell structure, which will provide a larger specific surface area and further improve the functional performance of the material. Shi and his colleagues[23] used polydopamine to coat and chelate MnO_2 on the surface of Fe_3O_4, which showed good adsorption properties for Pd.

Herein, an improved method has been used to modify Ag NPs on the PDA coating of Fe_3O_4@PDA NPs. In the synthesis process, Fe_3O_4 NPs provided a stable adhesive template for PDA to realize the formation of Fe_3O_4@PDA core–shell structure. Meanwhile, Fe_3O_4 NPs were superparamagnetic to ensure the fast and effective recovery of the material after the reaction was completed. PDA worked as both a support and a reducing agent at the same time. The synthetic process was green, pollution-free and did not involve additional reducing agent. It could effectively prevent the aggregation of silver nanoparticles and improve the catalytic cycle and stability of silver nanoparticles. At the same time, the surface of the material was negatively charged due to the presence of Ag NPs, which resulted in a good

[a]*School of Materials Science and Engineering, Jiangsu University of Science and Technology, Zhenjiang, 212100, China. E-mail: zhouhaijun@just.edu.cn*

[b]*Ministry of Education Key Laboratory of Advanced Civil Engineering Materials, School of Materials Science and Engineering, Tongji University, Shanghai, 201804, China. E-mail: ruiliu@tongji.edu.cn*

† Electronic supplementary information (ESI) available. See DOI: 10.1039/d1ra09187e

Open Access Article. Published on 31 January 2022. Downloaded on 8/14/2025 12:41:19 PM. This article is licensed under a Creative Commons Attribution-NonCommercial 3.0 Unported Licence.

Open Access Article. Published on 31 January 2022. Downloaded on 8/14/2025 12:41:19 PM.
This article is licensed under a Creative Commons Attribution-NonCommercial 3.0 Unported Licence.

selectivity and catalytic performance for other organic pollutants (MB and MO).

2. Materials and methods

2.1 Materials

Iron chloride hexahydrate ($FeCl_3 \cdot 6H_2O$), trisodium citrate dihydrate, ethylene glycol, sodium acetate anhydrous, dopamine, hydrochloric acid, sodium borohydride, silver nitrate, 4-nitrophenol (4-NP), methylene blue, and methyl orange were purchased from Sinopharm Chemical Reagent Co., Ltd. All chemicals were used as received.

2.2 Synthesis of Fe_3O_4 and Fe_3O_4@PDA

The synthesis of Fe_3O_4 and Fe_3O_4@PDA nanoparticles was carried out according to the following procedure.[24] Briefly, 1.08 g of ferric chloride hexahydrate ($FeCl_3 \cdot 6H_2O$) and 0.46 g of trisodium citrate were put into 40 ml of ethylene glycol to form a dispersed solution through stirred at room temperature. Then, 2.4 g of anhydrous sodium acetate was added to the above solution. The above mixed solution was stirred for half an hour and transferred to a closed polytetrafluoroethylene reactor, which took place for 12 h under a temperature of 200 °C. After completion of the reaction, the reactor was cooled to room temperature. The black precipitate was collected using a magnetic block and washed with deionized water and ethanol repeatedly. Then, the obtain black powder was dried under vacuum at 60 °C for 6 h. 40 mg of Fe_3O_4 particles and 120 mg of dopamine were uniformly dispersed in 50 ml of Tris–HCl (10 mM, pH = 8.5) solution. The reaction system was stirred for 3 hours at room temperature. The final product was obtained through separated magnetically and washed with deionized water and ethanol, then dried at 60 °C for 6 h in a vacuum oven.

2.3 Synthesis of Fe_3O_4@PDA@Ag nanoparticles

Briefly, 20 mg of Fe_3O_4@PDA nanoparticles were dispersed in 50 ml of silver nitrate (1 mM) aqueous. Then, the reaction was continued for 20 minutes under sonicating at room temperature. The final product was magnetically separated and washed with deionized water and ethanol for multiple times, and then dried in vacuum at 60 °C for 6 h.

2.4 Catalytic performance test

In order to investigate the catalytic performance of the obtained Fe_3O_4@PDA@Ag nanoparticles, we selected 4-NP as model molecules to characterize the process. In the catalytic experiments, fresh $NaBH_4$ (10 ml, 0.1 M) solution was added to 4-NP solution (20 ml, 0.1 mM) at room temperature. Fe_3O_4@PDA@Ag (10 mg) was added to 4-NP solution to catalyze the reduction reaction. The progress of this catalytic reaction was monitored using UV-vis spectroscopy at room temperature. For the next recycling experiment, the used Fe_3O_4@PDA@Ag nanoparticles was recovered by magnetic separation, and was then washed with deionized water and ethanol thoroughly several times. The catalytic process was repeated for 10 consecutive cycles using the same solid powder with new fresh 4-NP and $NaBH_4$ aqueous solution. The first-order kinetic equation was used to evaluate the catalytic performance of Fe_3O_4@PDA@Ag material for 4-NP:

$$-\ln(C_t/C_0) = kt$$

where C_0 and C_t were the concentrations of 4-NP at time 0 and t. The same method was used for the catalytic characterization of MB and MO.

2.5 Characterization

Transmission electron microscopy (TEM) images were obtained by JEM-2100F operated. Scanning electron microscope (SEM) images were obtained by Zeiss Merlin compact field emission with an accelerating voltage of 20 kV. The Fourier-transform infrared (FTIR) spectra were recorded on the Bruker Equinox 55 spectrometer in transmission mode. The scan range was from 4000 to 500 cm^{-1}. The magnetic properties of the products were characterized using a HH-20 VSM with an applied field between −1500 and 1500 Oe at room temperature. UV-vis absorption spectra were recorded on a UV-3600 spectrophotometer (Shimadzu, Japan). Zeta potentials were measured using the NanoBrook 90Plus Zeta nano grain sized analyzer (Brookhaven, USA). X-ray diffraction (XRD) patterns were analyzed on a XRD-6000 X-ray diffractometer (Shimadzu, Japan). X-ray photoelectron spectra (XPS) were recorded on Axis Ultra DLD system using Al Kα radiation.

3. Results and discussion

Fig. 1 illustrated the synthesis process of Fe_3O_4@PDA@Ag. Usually, Fe_3O_4@PDA was synthesized through mixing Fe_3O_4 NPs with Tris-buffer containing dopamine. Afterward, Fe_3O_4@PDA NPs entrapped satellite Ag were prepared through dispersing Fe_3O_4@PDA NPs in silver nitrate solution by ultrasonic treatment at room temperature. Compared with uncoated Fe_3O_4 (Fig. 2a), scanning electron microscopy (SEM) images

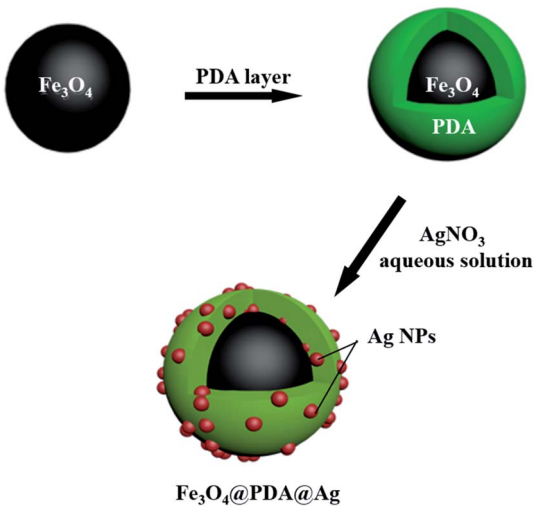

Fig. 1 Schematic illustration of formation procedure for Fe_3O_4@PDA@Ag.

© 2022 The Author(s). Published by the Royal Society of Chemistry

Open Access Article. Published on 31 January 2022. Downloaded on 8/14/2025 12:41:19 PM.
This article is licensed under a Creative Commons Attribution-NonCommercial 3.0 Unported Licence.

showed that the Fe_3O_4 NPs coated with PDA (Fig. 2d) have a smooth surface and a diameter of about 330 nm. Transmission electron microscopy (TEM) images (Fig. 2b) showed that the Fe_3O_4 NPs were close to spherical in shape and uniform in size with a diameter of ~305 nm with good dispersion. TEM images in Fig. 2e showed that Fe_3O_4@PDA NPs were uniformly spherical and the thickness of PDA shell was ~20 nm. Fe_3O_4@PDA@Ag NPs were obtained through ultrasonic stirring by dispersing Fe_3O_4@PDA NPs in aqueous silver nitrate solution without any additional reducing agent. TEM images of Fe_3O_4@PDA@Ag (Fig. 2g) showed that Ag NPs were deposited on the surface of the PDA shell and the lattice spacing was 0.241 nm (Fig. 2h). The Ag NPs coated with Fe_3O_4@PDA showed regular shape and uniform particle size with a diameter of approximately 14.7 nm (Fig. 2i).

X-ray diffraction (XRD) of Fe_3O_4 was recorded in Fig. 3a. Six peaks at 30.1°, 35.8°, 43.1°, 54.4°, 57.0° and 62.6° were corresponded to the (2 2 0), (3 1 1), (4 4 0), (4 2 2), (5 1 1) and (4 4 0) planes of Fe_3O_4 (JCPDS card no. 19-0629). XRD pattern (Fig. 3a) of Fe_3O_4@PDA@Ag confirmed the presence of Ag NPs. Four new peaks at 38.1°, 44.3°, 64.4° and 77.5° respectively were correspond to the (111), (200), (220) and (311) planes of Ag NPs (JCPDS card no. 04-0783). The VSM was recorded in Fig. 3b. Compared with 31.6 emu g^{-1} of pure Fe_3O_4, the magnetization of Fe_3O_4@PDA coated by PDA was 12.8 emu g^{-1}, which had a certain degree of decrease. The magnetization of Fe_3O_4@PDA@Ag after *in situ* reduction of Ag NPs was 9.8 emu g^{-1}. The decrease of magnetization had little effect on the magnetic recovery performance of Fe_3O_4@PDA@Ag. There was almost no remanence (Mr) and coercivity (Hc) and no obvious hysteresis

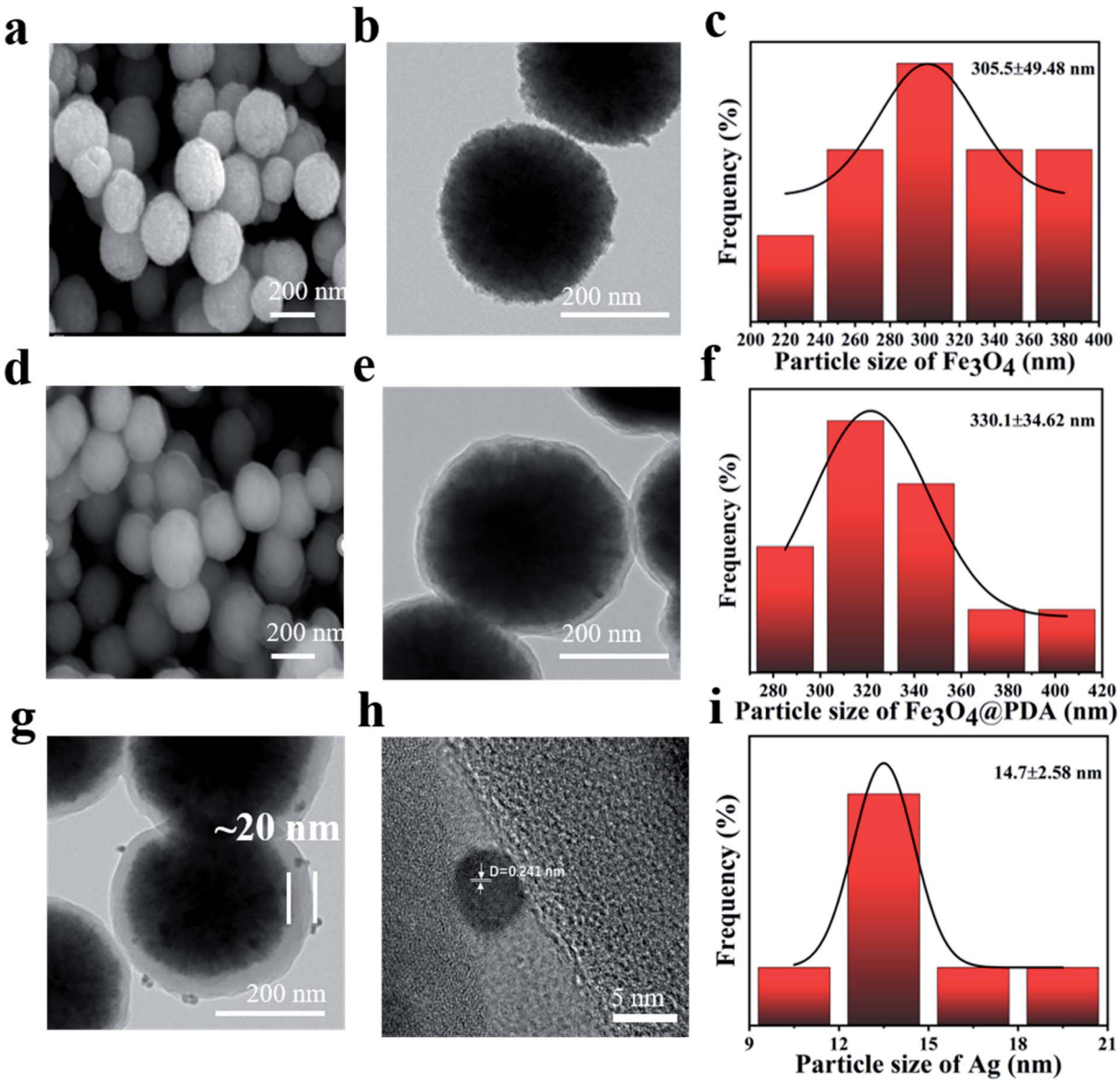

Fig. 2 SEM, TEM images and particle size of (a–c) Fe_3O_4, (d–f) Fe_3O_4@PDA core–shell NPs, (g and h) Fe_3O_4@PDA@Ag. (i) Particle size distribution of Ag NPs.

Open Access Article. Published on 31 January 2022. Downloaded on 8/14/2025 12:41:19 PM.
This article is licensed under a Creative Commons Attribution-NonCommercial 3.0 Unported Licence.

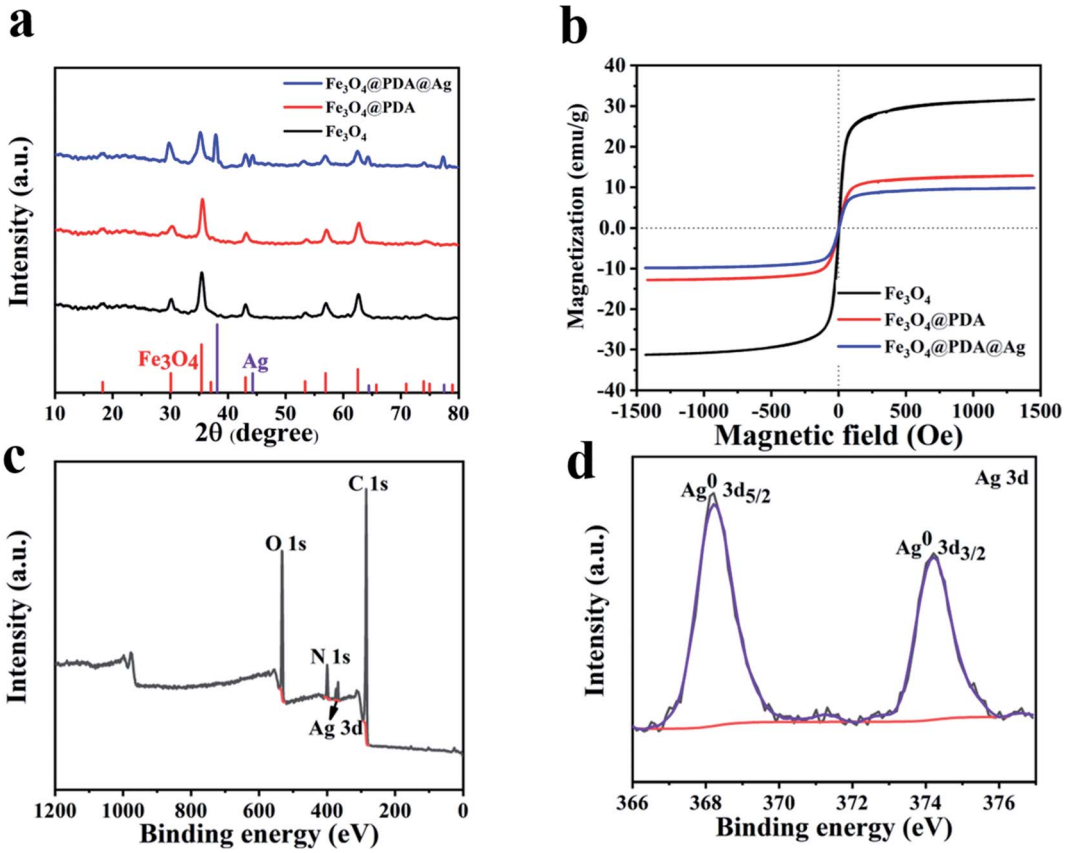

Fig. 3 (a) XRD patterns. (b) VSM of Fe_3O_4, Fe_3O_4@PDA and Fe_3O_4@PDA@Ag. (c) XPS of Fe_3O_4@PDA@Ag. (d) High-resolution XPS spectra of Ag 3d.

loop appeared on the VSM curve, indicating that the material has superparamagnetic properties.[25] Generally, Ag nanoparticles can be reduced and deposited on the surface of PDA by adding a reducing agent (such as sodium borohydride) or high temperature.[20,26] A remarkable feature of our reported synthesis method is that it abandons the long reaction time required for *in situ* reduction. Fe_3O_4@PDA@Ag nanoparticles obtained through fast preparation by ultrasonic treatment at room temperature. Silver ions in silver nitrate solution infiltrated into PDA layer, chelated and reduced to Ag NPs by phenol hydroxyl groups of PDA. Silver nanoparticles were deposited on the PDA layer. Therefore, in our work, PDA can be used not only as a carrier, but also as a reducing agent to reduce silver nitrate solution.

The Fourier infrared transform (FTIR) of Fe_3O_4, Fe_3O_4@PDA and Fe_3O_4@PDA@Ag were shown in Fig. S1.† Compared with pure Fe_3O_4, the increase of peak intensity at 1640 cm^{-1} was caused by aromatic ring on PDA. The broad peak at 3400 cm^{-1} was attributed to the hydroxyl group in the composite product.[27,28] Due to its instability, only a small amount of C=O remained after reduction. Infrared spectrum also confirmed the success of PDA cladding. The characteristic peak of hydroxyl in Fe_3O_4@PDA@Ag became weaker or even disappeared, indicating that part of phenolic hydroxyl was consumed by *in situ* reduction of silver particles. X-ray photoelectron spectroscopy (XPS) was used to confirm the elemental composition and surface chemical state of Fe_3O_4@PDA@Ag core–shell nanomaterials (Fig. 3c and d). In addition to the peaks of C, N, and O belonging to PDA in Fig. 3c, the Ag 3d peaks of Fe_3O_4@PDA@Ag in Fig. 3d were also assigned to Ag^0 at 368.2 and 374.9 eV.[29] The results showed that Ag existed in the polydopamine layer in the form of elemental silver, which might be used for catalytic applications.

The encapsulation of PDA on Fe_3O_4 could be analysed by TG test and the thermogravimetric curves of Fe_3O_4, Fe_3O_4@PDA@Ag were shown in Fig. 4. As shown in Fig. 4, the weight loss with increasing temperature up to 150 °C was caused by the evaporation of the water adsorbed in the sample. The weight loss of pure Fe_3O_4 NPs after 200 °C should be related to the organic solvent (*e.g.* trisodium citrate) involved in the preparation of residual Fe_3O_4, and when the temperature was further increased to 800 °C, the weight of pure Fe_3O_4 nanoparticles remained relatively stable and showed good thermal stability. For PDA, the weight loss was 20% by mass and this stage of weight loss corresponded to the decomposition and carbonisation of the polydopamine. When the temperature was further increased from around 400 °C to 800 °C, the Fe_3O_4@PDA nanomaterials showed good thermal stability.

The reduction of 4-nitrophenol (4-NP) to 4-aminophenol (4-AP) in the sodium borohydride system was used as a catalytic

© 2022 The Author(s). Published by the Royal Society of Chemistry

Open Access Article. Published on 31 January 2022. Downloaded on 8/14/2025 12:41:19 PM.
This article is licensed under a Creative Commons Attribution-NonCommercial 3.0 Unported Licence.

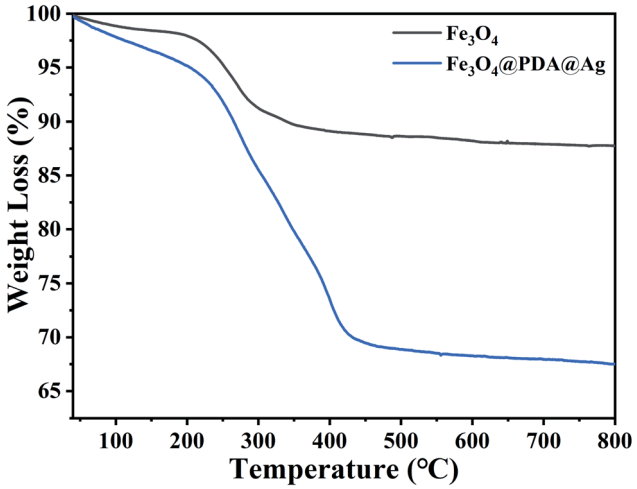

Fig. 4 TG curve of Fe_3O_4 and Fe_3O_4@PDA@Ag.

model to monitor and evaluate the catalytic performance of Fe_3O_4@PDA@Ag hybrid materials. As shown in Fig. 5a, the aqueous solution mixed with 4-NP (20 ml, 0.1 mM) and $NaBH_4$ (10 ml, 0.1 M) was bright yellow, and had nearly no change for a long time unless the catalyst was added. After adding the Fe_3O_4@PDA@Ag (10 mg) as a catalyst, the absorption peak of ~400 nm was significantly reduced, while the system solution changed from bright yellow to pale yellow to colorless simultaneously after only 4 minutes. After the catalysis was completed, Fe_3O_4@PDA@Ag was separated and recycled using a magnet. The UV-vis absorption spectrum of the solution was detected once a minute to monitor the progress of the reaction. Over time, 4-NP (~400 nm) absorbance dropped rapidly, while the absorbance of 4-AP (~295 nm) increased, and the reduction process was completed in about 4 minutes (Fig. 5b). As shown in Fig. 5c, there is a good linear relationship between $\ln(C_t/C_0)$ and reaction time, which proved that the reaction follows first-order kinetics. The calculated rate constant k at initial 0.1 mM 4-NP was 1.03 min^{-1}. Table 1 listed the comparison of catalytic performance of various catalysts, which showed that our reported catalyst exhibited a higher catalytic activity than that of other catalysts, including Fe_3O_4/SiO_2@Ag and Au/PMMA.[30–32] In order to verify that Ag was the focus of the catalytic activity in the hybrid material, a comparative experiment was carried out. Fe_3O_4 and Fe_3O_4@PDA were put into the catalytic system respectively. The results in Fig. S2† showed that the matrix material hardly had a catalytic effect on 4-NP in the absence of

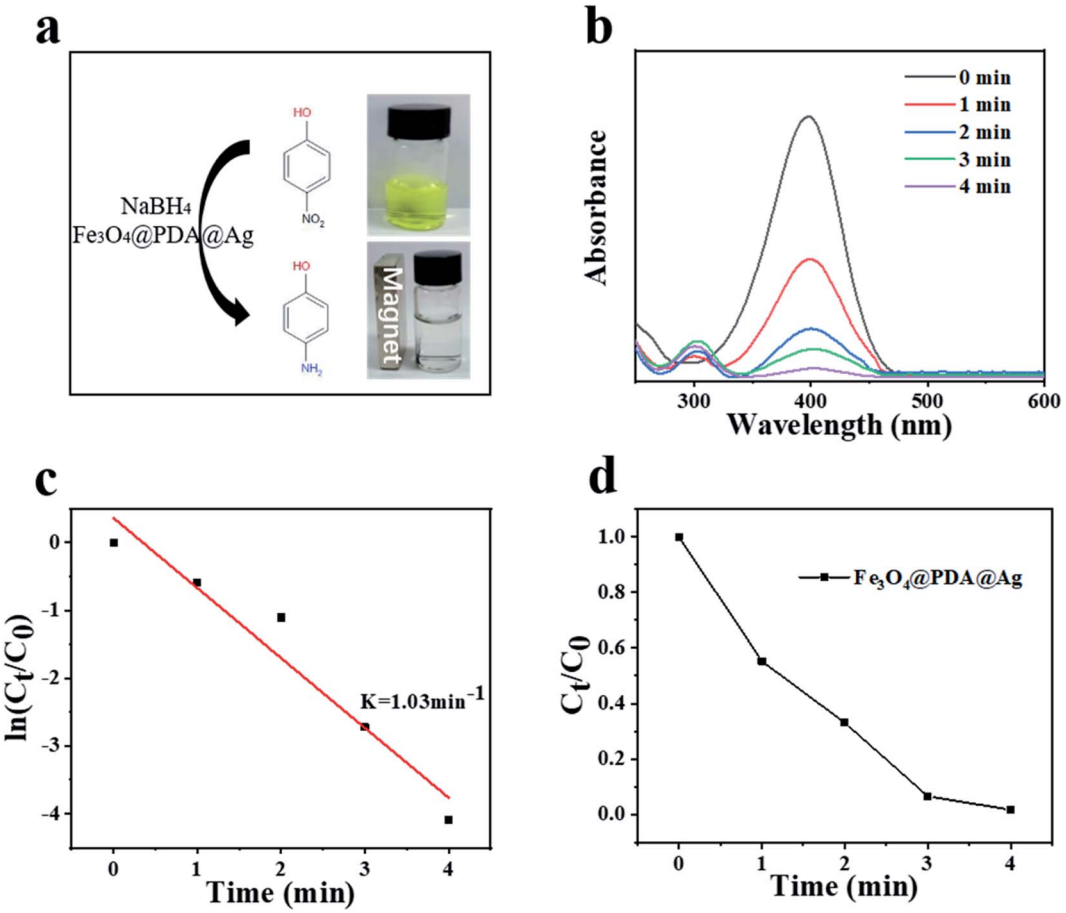

Fig. 5 (a) Reaction scheme and color change. (b) UV-vis spectra of different durations. (c) Plots of $\ln(C_t/C_0)$ against the reaction time. (d) Plots of C_t/C_0 against the reaction time.

Open Access Article. Published on 31 January 2022. Downloaded on 8/14/2025 12:41:19 PM.
This article is licensed under a Creative Commons Attribution-NonCommercial 3.0 Unported Licence.

Table 1 Comparison of the performance with other reported catalysts

Catalyst	$NaBH_4$/4-NP/catalyst mol mol^{-1}/1 mg	K (S^{-1})	Ref.
Fe_3O_4/SiO_2@Ag	$6.1 \times 10^{-4}/3.9 \times 10^{-7}/1$	0.0092	30
Au/PMMA	$5 \times 10^{-6}/2.5 \times 10^{-8}/1$	0.0055	31
Ag_2S NPs/RGO	$5 \times 10^{-5}/6 \times 10^{-8}/1$	0.0072	33
Fe_3O_4@SiO_2–Au@mSiO_2	$6.7 \times 10^{-5}/1.7 \times 10^{-7}/1$	0.0058	34
Fe_3O_4/PDA/Ag	$6.7 \times 10^{-5}/1 \times 10^{-7}/1$	0.0170	This work

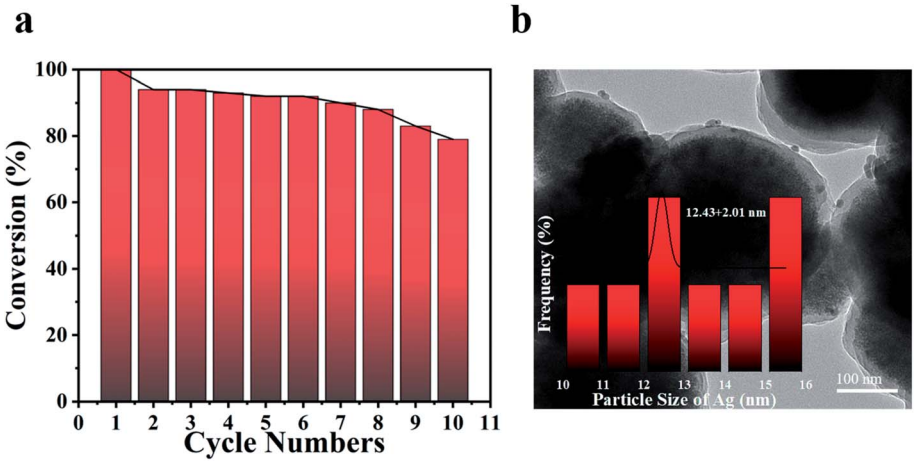

Fig. 6 (a) Catalytic reuse efficiency of Fe_3O_4@PDA@Ag. (b) TEM of catalyst after 10 cycles.

nano-silver. TEM of all silver-loaded samples were also shown in Fig. S3.†

The stability and cycling ability of Fe_3O_4@PDA@Ag were tested by reusing the same catalytic process for 10 times. The catalyst Fe_3O_4@PDA@Ag in this work was able to be recovered effectively from the reaction solution by magnetic adsorption for many cycles. As shown in Fig. 6a, Fe_3O_4@PDA@Ag still displayed surprisingly high activity after ten cycles, and the conversion rate was almost higher than 80% in about 10 minutes. After 10 cycles, the conversion decreased slightly by 20%, which might be attributed to the shedding of Ag NP in the process of cyclic catalysis. The TEM image (Fig. 6b) showed that Ag NPs (~12.43 nm) were still well dispersed in the polydopamine layer even after multiple recycles, which indicates that the polydopamine layer could be effectively used as a carrier to stabilize multiple Ag NPs. The excellent catalytic performance and reusability were believed to come from synergistic effect of Fe_3O_4@PDA@Ag: (1) Ag NPs were effectively fixed within the stable polydopamine layer, avoiding aggregation after reaction; (2) the deposited silver nanoparticles ensured high catalytic activity; (3) the effective magnetic separation prevented loss of the catalyst and allowed easy collection, thereby improving the reusability.

In addition, the selectivity of the catalyst Fe_3O_4@PDA@Ag was also studied for other organic dyes. As shown in Fig. 7a and c, Fe_3O_4@PDA@Ag exhibited quick catalytic reduction for MO and MB. There was a good linear relationship between $\ln(C_t/C_0)$ and reaction time, as shown in Fig. 7b and d, which proved that the reaction followed first-order kinetics. The catalytic rates for MO and MB are 0.47 min^{-1} and 0.61 min^{-1}, respectively. The zeta potential of Fe_3O_4@PDA@Ag was −28.9 mV. The results showed that the catalytic difference between the anionic dye MO and the cationic dye MB was caused by the negative potential of Ag NPs on the surface of the catalyst Fe_3O_4@PDA@Ag.[35] For the cationic dye MB, the electrostatic attraction between the materials can make MB quickly accumulate on the surface of Ag NPs, which promoted the catalytic reaction and accelerated the catalytic rate of Fe_3O_4@PDA@Ag on MB.

4. Conclusions

In this work, a simple and effective method was explored to synthesize Fe_3O_4@PDA core shell NPs-encapsulated silver nanocatalysts. The Ag NPs were encapsulated in the Fe_3O_4@PDA shell layer by using PDA as a carrier and reducing agent. Fe_3O_4@PDA@Ag NPs exhibited enhanced catalytic performance towards the reduction of 4-nitrophenol. After several catalytic cycles, the obtained Fe_3O_4@PDA@Ag NPs still maintained structural integrity and efficient catalytic activity. At the same time, Fe_3O_4@PDA@Ag NPs exhibited enhanced catalytic performance and selectivity to MB and MO. This simple and green synthesis method enabled the rapid decoration of tiny Ag

© 2022 The Author(s). Published by the Royal Society of Chemistry

Open Access Article. Published on 31 January 2022. Downloaded on 8/14/2025 12:41:19 PM.
This article is licensed under a Creative Commons Attribution-NonCommercial 3.0 Unported Licence.

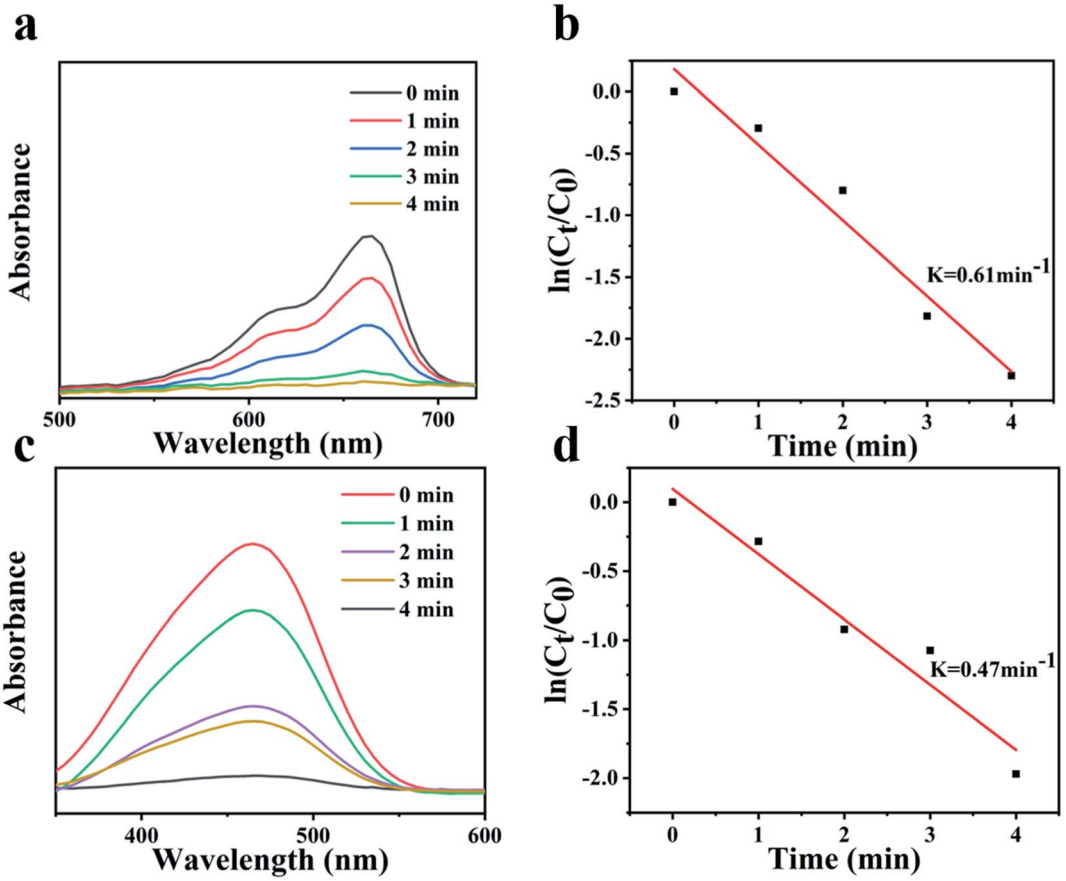

Fig. 7 UV-vis spectra of (a) MB and (b) MO with various durations. Plots of $\ln(C_t/C_0)$ against the reaction time for (c) MB and (d) MO.

NPs with Fe_3O_4@PDA core–shell nanoparticles and would provide a platform for other catalytic applications.

Conflicts of interest

There are no conflicts to declare.

Acknowledgements

We greatly appreciate the financial supports of National Natural Science Foundation of China (No. 51903111), Postgraduate Research & Practice Innovation Program of Jiangsu Province (KYCX21_3457).

References

1 Y. Mao, J. Xu and C. Ma, A continuous microwave/nZVI treatment system for malachite green removal: system setup and parameter optimization, *Desalin. Water Treat.*, 2016, **57**, 24395–24405.
2 M. Ahmaruzzaman and S. L. Gayatri, Batch adsorption of 4-nitrophenol by acid activated jute stick char: Equilibrium, kinetic and thermodynamic studies, *Chem. Eng. J.*, 2010, **158**, 173–180.
3 J. Pan and B. Guan, Adsorption of nitrobenzene from aqueous solution on activated sludge modified by cetyltrimethylammonium bromide, *J. Hazard. Mater.*, 2010, **183**, 341–346.
4 F. Nawaz, Y. Xie, H. Cao, J. Xiao, Y. Q. Wang, X. Zhang, M. Li and F. Duan, Catalytic ozonation of 4-nitrophenol over an mesoporous α-MnO_2 with resistance to leaching, *Catal. Today*, 2015, **258**, 595–601.
5 D. Kalaimurugan, P. Sivasankar, K. Durairaj, M. Lakshmanamoorthy, S. Ali Alharbi, S. A. Al Yousef, A. Chinnathambi and S. Venkatesan, Novel strategy for biodegradation of 4-nitrophenol by the immobilized cells of Pseudomonas YPS_3 with Acacia gum, *Saudi J. Biol. Sci.*, 2021, **28**, 833–839.
6 K. Sahu, J. Singh and S. Mohapatra, Catalytic reduction of 4-nitrophenol and photocatalytic degradation of organic pollutants in water by copper oxide nanosheets, *Opt. Mater.*, 2019, **93**, 58–69.
7 D. Motta, F. Sanchez, K. Alshammari, L. E. Chinchilla, G. A. Botton, D. Morgan, T. Tabanelli, A. Villa, C. Hammond and N. Dimitratos, Preformed Au colloidal nanoparticles immobilised on NiO as highly efficient heterogeneous catalysts for reduction of 4-nitrophenol to 4-aminophenol, *J. Environ. Chem. Eng.*, 2019, **7**, 263–275.

© 2022 The Author(s). Published by the Royal Society of Chemistry

Open Access Article. Published on 31 January 2022. Downloaded on 8/14/2025 12:41:19 PM.
This article is licensed under a Creative Commons Attribution-NonCommercial 3.0 Unported Licence.

8 A. Kalenchuk, V. Bogdan, S. Dunaev and L. Kustov, Influence of steric factors on reversible reactions of hydrogenation-dehydrogenation of polycyclic aromatic hydrocarbons on a Pt/C catalyst in hydrogen storage systems, *Fuel*, 2020, **280**, 118625–118634.

9 S. Gu, Y. Lu and J. Kaiser, Kinetic analysis of the reduction of 4-nitrophenol catalyzed by Au/Pd nanoalloys immobilized in spherical polyelectrolyte brushes, *Phys. Chem. Chem. Phys.*, 2015, **17**, 28137–28143.

10 S. Naraginti and A. Sivakumar, Eco-friendly synthesis of silver and gold nanoparticles with enhanced bactericidal activity and study of silver catalyzed reduction of 4-nitrophenol, *Spectrochim. Acta, Part A*, 2014, **128**, 357–362.

11 P. Liu and M. Zhao, Silver nanoparticle supported on halloysite nanotubes catalyzed reduction of 4-nitrophenol (4-NP), *Appl. Surf. Sci.*, 2009, **255**, 3989–3993.

12 W. Yang, W. Hu, J. Zhang, W. Wang, R. Cai, M. Pan, C. Huang, X. Chen, B. Yan and H. Zeng, Tannic acid/Fe^{3+} functionalized magnetic graphene oxide nanocomposite with high loading of silver nanoparticles as ultra-efficient catalyst and disinfectant for wastewater treatment, *Chem. Eng. J.*, 2020, **405**, 126629–126637.

13 I. B. Laskar, L. Rokhum, R. Gupta and S. Chatterjee, Zinc oxide supported silver nanoparticles as a heterogeneous catalyst for production of biodiesel from palm oil, *Environ. Prog. Sustainable Energy*, 2019, **39**, 13369–13374.

14 S. Ghiassi, M. Mokhtary, S. Sedaghat and H. Kefayati, Preparation and Antibacterial Activity of Chloroacetic Acid Immobilized on Chitosan Coated Iron Oxide Decorated Silver Nanoparticles as an Efficient Catalyst for the Synthesis of Hexahydroquinoline-3-Carboxamides, *J. Inorg. Organomet. Polym. Mater.*, 2019, **29**, 1972–1982.

15 M. N. Khrizanforov, S. V. Fedorenko, A. R. Mustafina, K. V. Kholin, I. R. Nizameev, S. O. Strekalova, V. V. Grinenko, T. V. Gryaznova, R. R. Zairov, R. Mazzaro, V. Morandi, A. Vomiero and Y. H. Budnikova, Silica-supported silver nanoparticles as an efficient catalyst for aromatic C-H alkylation and fluoroalkylation, *Dalton Trans.*, 2018, **47**, 9608–9616.

16 T. Y. Ying, A. A. A. Raman, M. M. Bello and A. Buthiyappan, Magnetic graphene oxide-biomass activated carbon composite for dye removal, *Korean J. Chem. Eng.*, 2020, **372**, 2179–2191.

17 E. Samuel, B. Joshi, C. Park, A. Aldalbahi, M. Rahaman and S. S. Yoon, Supersonically sprayed rGO/ZIF8 on nickel nanocone substrate for highly stable supercapacitor electrodes, *Electrochim. Acta*, 2020, **362**, 137154–137162.

18 G. Zhu, Y. Qi, F. Liu, S. Ma, G. Xiang, F. Jin, Z. Liu and W. Wang, Reconstructing 1D Fe single-atom catalytic structure on 2D graphene film for high-efficiency oxygen reduction reaction, *ChemSusChem*, 2020, **126**, 142–147.

19 Z. Zhai, Q. Wu, J. Li, B. Zhou, J. Shen, Z. H. Farooqi and W. Wu, Enhanced catalysis of gold nanoparticles in microgels upon on site altering the gold-polymer interface interaction, *J. Catal.*, 2019, **369**, 462–468.

20 C. Gong, Z. Zhou, H. Zhou and R. Liu, Vacuum-assisted synthesis of tiny Au nanoparticles entrapped into mesoporous carbon matrix with superior catalytic activity for 4-nitrophenol reduction, *Adv. Powder Technol.*, 2019, **30**, 649–655.

21 J. Chen, J. Qi, R. Liu, X. Zhu, Z. Wan, Q. Zhao, S. Tao, C. Dong, G. Y. Ashebir, W. Chen, R. Peng, F. Zhang, S. Yang, X. Tian and M. Wang, Preferentially oriented large antimony trisulfide single-crystalline cuboids grown on polycrystalline titania film for solar cells, *Commun. Chem.*, 2019, **2**, 121–128.

22 K. Wang, D. W. Sun, H. Pu and Q. Wei, Polymer multilayers enabled stable and flexible Au@Ag nanoparticle array for nondestructive SERS detection of pesticide residues, *Talanta*, 2021, **223**, 121782–121795.

23 S. Shi, C. Xu, Q. Dong, Y. Wang, S. Zhu, X. Zhang, Y. Tak Chow, X. Wang, L. Zhu, G. Zhang and D. Xu, High saturation magnetization MnO_2/PDA/Fe_3O_4 fibers for efficient Pb(II) adsorption and rapid magnetic separation, *Appl. Surf. Sci.*, 2020, **541**, 148379–148386.

24 S. Xuan, Y. X. J. Wang, J. C. Yu and K. Cham-Fai Leung, Tuning the grain size and particle size of superparamagnetic Fe_3O_4 microparticles, *Chem. Mater.*, 2009, **21**, 5079–5084.

25 C. Gong, Q. Li, H. Zhou and R. Liu, Tiny Au satellites decorated Fe_3O_4@3-aminophenol-formaldehyde core-shell nanoparticles: Easy synthesis and comparison in catalytic reduction for cationic and anionic dyes, *Colloids Surf., A*, 2018, **540**, 67–72.

26 C. Gong, Z. Zhou, J. Li, H. Zhou and R. Liu, Facile synthesis of ultra stable Fe_3O_4 @Carbon core-shell nanoparticles entrapped satellite au catalysts with enhanced 4-nitrophenol reduction property, *J. Taiwan Inst. Chem. Eng.*, 2018, **7**, 229–235.

27 J. Zhao, R. Luque, W. Qi, J. Lai, W. Gao, M. R. Hasan Shah Gilani and G. Xu, Facile surfactant-free synthesis and characterization of Fe_3O_4@3-aminophenol-formaldehyde core-shell magnetic microspheres, *J. Mater. Chem. A*, 2015, **3**, 519–524.

28 C. Gong, Z. Zhou, R. Liu and H. Zhou, Facile Synthesis of Gold Nanoparticles Decorated Core-Shell Fe_3O_4@Carbon: Control of Surface Charge and Comparison in Catalytic Reduction for Methyl Orange, *J. Nanosci. Nanotechnol.*, 2020, **20**, 2330–2336.

29 S. S. Chen, H. Xu, H. J. Xu, G. J. Yu, X. L. Gong, Q. L. Fang, K. C. Leung, S. H. Xuan and Q. R. Xiong, A facile ultrasonication assisted method for Fe_3O_4@SiO_2-Ag nanospheres with excellent antibacterial activity, *Dalton Trans.*, 2015, **44**, 9140–9148.

30 K. Kuroda, T. Ishida and M. Haruta, Reduction of 4-nitrophenol to 4-aminophenol over Au nanoparticles deposited on PMMA, *J. Mol. Catal. A: Chem.*, 2009, **298**, 7–11.

31 L. Zhang, J. P. Thomas, X. Guan, N. F. Heinig and K. T. Leung, High-energy ion (He(+), Si(++), Ga(+), Au(++)) interactions with PMMA in ion beam lithography, *Nanotechnology*, 2020, **31**, 325301–325312.

32 C. Gong, Z. Zhou, H. Zhou and R. Liu, Vacuum-assisted synthesis of tiny Au nanoparticles entrapped into mesoporous carbon matrix with superior catalytic activity for 4-nitrophenol reduction, *Adv. Powder Technol.*, 2019, **30**, 649–655.

© 2022 The Author(s). Published by the Royal Society of Chemistry

Open Access Article. Published on 31 January 2022. Downloaded on 8/14/2025 12:41:19 PM.
This article is licensed under a Creative Commons Attribution-NonCommercial 3.0 Unported Licence.

33 Z. Mo, P. Liu, R. Guo, Z. Deng, Y. Zhao and Y. Sun, Graphene sheets/Ag_2S nanocomposites: Synthesis and their application in supercapacitor materials, *Mater. Lett.*, 2012, **68**, 416–418.
34 Y. H. Deng, Y. Cai, Z. K. Sun and J. Liu, Multifunctional mesoporous composite microspheres with well-designed nanostructure: A highly integrated catalyst system, *American Chemical Society*, 2010, **132**, 8466–8473.
35 S. M. Mohd Yasin, I. A. Badruddin and M. R. Johan, Super stability of Ag nanoparticle in crystalline lamellar (Lc) liquid crystal matrix at different pH environment, *Symmetry*, 2019, **12**, 31–37.

© 2022 The Author(s). Published by the Royal Society of Chemistry